ELSEVIER

Applied Ocean Research 25 (2003) 1–19

Applied Ocean Research

www.elsevier.com/locate/apor

Estimating nonlinear coupled frequency-dependent parameters in offshore engineering

P.F. Liagre, J.M. Niedzwecki*

Department of Civil Engineering, Texas A&M University, Engineering Program Office, 301 Wisenbaker Engineering Research Centre, College Station, TX 77843, USA

Received 1 November 2002; revised 4 April 2003; accepted 4 April 2003

Abstract

The design of deepwater compliant offshore structures requires engineers to address many difficult challenges including defining and modeling the local offshore environment, specifying the associated combined global loading on innovative platform designs, and numerical simulation and model test verification of the platform response characteristics. The focus of this research investigation is the recovery of key parameters from time series measured during an industry type model basin test program using the reverse multiple input/single output technique. In particular, this study confronts critical problems of practical interest and extends the methodology to address the inclusion of nonlinear coupled systems in which the parameters of interest can be frequency-dependent. The analysis is developed around the nonlinear coupled equations of motions for a deepwater mini-TLP design and includes the consideration of nonlinear stiffness, quadratic damping, surge/pitch and sway/roll coupling and the frequency dependency of both the hydrodynamic added-mass and damping coefficients. A series of complementary model test measurements for the complete compliant model and the rigidly restrained hull by itself were used as the basis for the data in the system identification procedures. In addition, behavior of the hydrodynamic added-mass and damping coefficients as a function of frequency was simulated for the mini-TLP using an industry standard radiation–diffraction software package. These results were used in evaluating the accuracy of some of the key problem parameters. The results presented demonstrate the methodology as modified in this study is quite robust and yields predications that are more accurate for the parameters associated with the largest motions of the platform. Practical issues regarding the application of this approach, utilization of both force and moment measurements, and observed strengths and weakness in dealing with data regardless of its source are discussed.

Keywords: System identification; Multiple input/single output problem; MATLAB; WAMIT; Frequency-dependent parameters; Nonlinear equations; Coupled equations; Hydrodynamic added-mass; Hydrodynamic damping; Mini-TLP; Deepwater platform response

1. Introduction

The reverse multiple input/single output (R-MI/SO) technique as originally developed by Bendat [1,2] and Bendat et al. [3] is a frequency domain system identification technique that is suited to address a wide range of problems in science and engineering. The methodology, which is intended to extract information about the system parameters directly from recorded time series, requires measurement of the excitation (cause) and the corresponding response data (effect). In the formulation the causality is reversed, meaning that the system kinematics (displacements, velocities, etc.) that are typically the output due to the applied loading inputs (forces and moments) are switched, that is the outputs become the inputs and vice versa. A conditioning procedure is then applied to successively eliminate the linear contents between the inputs and the output. These operations decompose the nonlinear system into a number of linear sub-systems. The auto- and cross-spectra are used to obtain the linear transfer functions of each sub-system, and subsequently by examining these transfer functions and the ordinary and cumulative coherence functions for each linear and nonlinear term, one can interpret the importance and magnitudes of the desired system parameters. It is worth noting here that should additional nonlinear terms be introduced into the problem definition, the procedure will yield coefficients whose value is essentially zero and effectively the terms will drop out. This method is therefore particularly

* Corresponding author. Tel.: +1-979-862-1463; fax: +1-979-845-8986.
E-mail address: j-niedzwecki@tamu.edu (J.M. Niedzwecki).

0141-1187/03/$ - see front matter © 2003 Elsevier Ltd. All rights reserved.
doi:10.1016/S0141-1187(03)00029-4

well suited for the identification of parameters appearing in nonlinear second-order differential equations of motion with constant or frequency-dependent coefficients, which are commonly encountered in offshore mechanics. The R-MI/SO method has been applied to single-degree-of-freedom (DOF) models of compliant offshore platform [11] and more recently to a nonlinear distributed-parameter multi-DOF model of a deepwater production riser [13].

In previous studies of fluid-structure interaction problems [6,15,16], computer-generated numerical data from simulated nonlinear systems were used to demonstrate that the R-MI/SO technique provides an accurate practical method to identify the dynamic properties of various desired nonlinear systems by converting nonlinear models into equivalent linear models. These studies were quite focused and did not take complete advantage of the R-MI/SO technique to help identify the best nonlinear integrodifferential equation of motion. Attention was directed at specified constant parameters used to synthesize the systems' dynamic response where the identified system parameters were numerically estimated from the spectral mean of the transfer functions over a determined frequency range, such as, the response frequency range of the system. Using a more extended approach, Bhattacharyya and Panneer Selvam [4] applied the R-MI/SO to a synthesized dataset describing the response of a large moored floating body to ocean waves, which included frequency-dependent added-mass and damping coefficients as well as linear and nonlinear mooring line stiffness coefficients. The application of the R-MI/SO method to a two input/single output model of the system showed that the recovery of the added-mass coefficient's frequency dependence is feasible and reasonably accurate as long as the linear stiffness coefficient is assumed to be constant. The frequency dependence of the damping coefficient was recovered quite accurately.

This study builds upon the R-MI/SO method as presently reported in the open literature but develops the methodology to address realistic systems with both constant and frequency-dependent parameters. Of particular interest is the identification of the frequency dependence of the hydrodynamic added-mass and damping coefficients, since these coefficients are essential for understanding of the nonlinear effects influencing the dynamic behavior of compliant deepwater offshore structures. Large-scale model test data from a recent model test program of a mini-TLP [8,14,18] is used as the basis to investigate the application of the R-MI/SO method. This model test data was selected since it contains data on both rigidly restrained hull and the corresponding compliant platform under identical wave conditions. This data set was selected for this reason, since it is impractical to measure the forces acting on a compliant structure without affecting its motions. The validity of assuming equivalency of forces and moments is investigated and discussed. The wave forces and moments were measured directly on the rigidly restrained hull model using a six DOF load cell. An infrared optical tracking system was used to monitor the compliant model response behavior. Again, each model was subjected to the same wave conditions. The restoring forces due to the vertical mooring system, the tendons, also commonly referred to as tethers, and risers were post-computed from the time series recordings of the mini-TLP motions.

Given that the tests used uni-directional wave excitation, only the parameters related to the dominant motions of surge, pitch and heave, and their coupling is considered. These motions directly affect the prevailing requirement for minimal response motion during platform operational time. Unlike the previous studies, the displacements and accelerations are used as two independent mathematical inputs to the equivalent R-MI/SO model in order to obtain two separate transfer functions yielding individual values for the mass plus added-mass and linear stiffness terms. No assumptions regarding the mathematical properties of the parameters are made during the analysis; the results presented are obtained directly from the procedures described and the trends are explained in terms of physical effects. Comparisons of the results obtained with different wave conditions are carried out with the objective of checking the consistency of the method. An industry standard nonlinear radiation–diffraction program [18,19] was used to evaluate the added-mass and damping coefficients for all modes as well as the added-mass coefficients for the limiting cases of zero or infinite wave periods. These computational predictions are used to confirm the accuracy of the R-MI/SO predictions as developed in this study.

2. Problem formulation

2.1. Nonlinear system of equations

Commonly, the first issue in the implementation of any system identification technique is the selection of the governing equation or equations. The selection of the appropriate mathematical model must reflect both physical insight and the known mechanical properties of the system. In the present study, Newton's second law of motion governs the mini-TLP motions and the choice of a nonlinear second-order differential equation of motion asserts itself naturally [6,12]. A nonlinear stiffness (Duffing) term as well as a nonlinear damping term is added to this equation in order to take into account the nonlinear restoring forces due to the vertical mooring system and the hydrodynamic damping due to the wave-structure interactions. The system of coupled nonlinear differential equations governing the six DOF mini-TLP motions can be expressed as

$$[M+A]\ddot{q}(t)+B\dot{q}(t)+Kq(t)+Rq^3(t)+D\dot{q}(t)|\dot{q}(t)|=f(t) \quad (1)$$

where M is the mass matrix, A is the hydrodynamic added-mass matrix, B is the linear damping matrix, K is

the linear stiffness matrix, R is a nonlinear Duffing type stiffness matrix, and D, the nonlinear damping matrix. The nonlinearity of the horizontal plane restoring forces due to the mooring system is accounted for by the cubic term. This first odd nonlinear function captures the change of direction of the restoring forces when surge or sway motions change of sign. The vertical restoring forces are believed to be dominated by linear behavior.

The general kinematic and environmental excitation vectors are defined as

$$q(t) = [x(t), y(t), z(t), \phi(t), \theta(t), \psi(t)]^T$$

$$q^3(t) = [x^3(t), y^3(t), z^3(t), \phi^3(t), \theta^3(t), \psi^3(t)]^T$$

$$\dot{q}(t)|\dot{q}(t)| = [\dot{x}(t)|\dot{x}(t)|, \dot{y}(t)|\dot{y}(t)|, \dot{z}(t)|\dot{z}(t)|, \dot{\phi}(t)|\dot{\phi}(t)|, \dot{\theta}(t)|\dot{\theta}(t)|, \dot{\psi}(t)|\dot{\psi}(t)|]^T \quad (2)$$

$$f(t) = [f_x(t), f_y(t), f_z(t), m_x(t), m_y(t), m_z(t)]^T$$

For each DOF [2], the components of $q(t)$, $q^3(t)$ and $\dot{q}(t)|q(t)|$ are taken as the inputs of the equivalent R-MI/SO model, while the component of $f(t)$ is taken as the output of the mathematical model. The platform kinematics vector, $q(t)$, encompasses the following translation and rotational components: $x(t)$ the surge motion response (inline), $y(t)$ the sway motion (transverse), $z(t)$ the heave motion (vertical), $\phi(t)$ the roll rotation response about the x axis, $\theta(t)$ the pitch rotation response about the y axis, and $\psi(t)$ the yaw rotation response about the z axis. The general excitation vector $f(t)$ contains the following total external forces and moments applied on the hull of the compliant mini-TLP: $f_x(t)$ the inline force excitation, $f_y(t)$ the transverse force excitation, $f_z(t)$ the vertical force excitation, $m_x(t)$ the roll moment excitation, $m_y(t)$ the pitch moment excitation and $m_z(t)$ the yaw moment excitation.

The matrices M, A, B, K, R, and D are each 6×6 matrices and except for the system mass matrix all the other matrices could be considered to be potentially frequency-dependent. The platform has two planes of symmetry and the origin of the axes on the platform is assumed to coincide with the center of gravity of the platform. Therefore the mass matrix, M, is a diagonal matrix. The first three entries on the diagonal are equal to the system structural mass, m, and the last three entries are the principal moments of inertia about the x, y and z axes, denoted I_{xx}, I_{yy} and I_{zz}, respectively.

In each problem being analyzed, each potential source of coupling between the degrees-of-freedom in the mathematical model must be considered and only the most significant terms are generally retained for analyses. A study of an unrestrained ship [10] concluded that all six-degrees of motion affect one another at least quantitatively, and in some cases qualitatively. Unlike free-floating vessels, TLP platforms have well-defined couplings between certain degrees-of-freedom, due to the platform geometry and vertical taut mooring system design. For the mini-TLP, based upon the geometrical and mooring system restraints, it could be anticipated that the most significant sources of motion coupling expected could include surge/heave, surge/pitch, sway/roll and heave/pitch. However, through further investigation of the model test data it was concluded that the surge/heave and heave/pitch coupling terms could be neglected for this particular platform, and only the coupling corresponding to the terms associated with the surge/pitch and sway/roll will be included in this study. More specifically, this will be reflected in the added-mass, linear damping and linear stiffness matrices. For a symmetric platform such as the mini-TLP, neglecting the second-order terms will result in the nonlinear stiffness matrix, R, and the nonlinear damping matrix, D, being diagonal matrices.

2.2. Equivalent reverse dynamics input/output models

The system of coupled nonlinear differential equations presented in Eq. (1) can be rewritten in the following indicial form

$$m_{ii}\ddot{q}_i(t) + \sum_{n=1}^{6} [a_{in}\ddot{q}_n(t) + b_{in}\dot{q}_n(t) + k_{in}q_n(t)] + r_{ii}q_i^3(t) + d_{ii}\dot{q}_i(t)|\dot{q}_i(t)| = f_i(t) \quad (3)$$

with $i = 1, 2, \ldots, 6$.

Upon taking the Fourier transform of both sides of Eq. (3), the equivalent mathematical reverse dynamics input/output models are obtained

$$\underbrace{H_i^l(\omega)U_i(\omega)}_{\text{Linear terms}} + \underbrace{\sum_{\substack{n=1 \\ n\neq i}}^{6} H_n^c(\omega)U_n(\omega)}_{\text{Linear coupling terms}} + \underbrace{H_i^r(\omega)V_i(\omega)}_{\text{Nonlinear stiffness}} + \underbrace{H_i^d(\omega)W_i(\omega)}_{\text{Nonlinear damping}} = F_i(\omega) \quad (4)$$

where $i = 1, 2, \ldots, 6$, and

$$U_i(\omega) = \Im[q_i(t)]$$

$$V_i(\omega) = \Im[q_i^3(t)] \quad (5)$$

$$W_i(\omega) = \Im[\dot{q}_i(t)|\dot{q}_i(t)|]$$

$$F_i(\omega) = \Im[f_i(t)]$$

In addition, $\omega = 2\pi f$, is the radian frequency, f is the frequency in Hz, and $\Im[\,]$ indicates a Fourier transform of the quantity in brackets. The relations between the transfer functions, H, and the Fourier transforms of the system parameters are found to be of the form

$$H_i^l(\omega) = K_{ii}(\omega) - \omega^2(M_{ii} + A_{ii}(\omega)) + j\omega B_{ii}(\omega) \quad (6)$$

$$H_n^c(\omega) = K_{in}(\omega) - \omega^2 A_{in}(\omega) + j\omega B_{in}(\omega) \quad (7)$$

$$H_i^r(\omega) = R_{ii}(\omega) \tag{8}$$

$$H_i^d(\omega) = D_{ii}(\omega) \tag{9}$$

The Fourier transforms $B_{ii}(\omega)$ and $B_{in}(\omega)$ of the linear damping coefficients b_{ii} and b_{in} appear by themselves, respectively, in the imaginary part of the transfer functions $H_i^l(\omega)$ and $H_n^c(\omega)$. Likewise, the Fourier transforms $R_{ii}(\omega)$ and $D_{ii}(\omega)$ of the nonlinear stiffness coefficients r_{ii} and nonlinear damping coefficients d_{ii} are found in the real part of two different transfer functions $H_i^r(\omega)$ and $H_i^d(\omega)$. This does not cause a problem for their evaluation from the transfer functions. However, the Fourier transforms $M_{ii}(\omega)$, $A_{ii}(\omega)$ and $K_{ii}(\omega)$, as well as $A_{in}(\omega)$ and $K_{in}(\omega)$, of the elements of the mass matrix M, the added-mass matrix A and linear stiffness matrix K turn up, respectively, in the real parts of the transfer functions $H_i^l(\omega)$ and $H_n^c(\omega)$. To avoid the problem of partitioning the structural system mass, the hydrodynamic added-mass and the linear stiffness terms, the formulation is modified in the following way. The acceleration and displacement signals are used as separate inputs. Given that the velocity is automatically accounted for by the imaginary part of the transfer function associated with the displacement, it does not need to be used as an input. Since the acceleration and displacement input signals are highly correlated, i.e. the acceleration is the second derivative with respect to time of the displacement; a method was developed to reduce the input signals' correlation before applying the conditioning procedure. Hence the mass appears alone in a dedicated transfer function, while the linear stiffness and linear damping appear, respectively, in the real and imaginary part of the second transfer function.

2.3. Analysis issues and solution paradigm

The most general equivalent mathematical reverse dynamics multiple input/multiple output (MI/MO) linear model has 24-inputs, the original six physical inputs $q(t)$ with its second derivative $\ddot{q}(t)$, plus the six associated $q^3(t)$ terms and the six associated $\dot{q}(t)|\dot{q}(t)|$ terms, and six outputs, the original three physical forces and the three physical moments. Whenever possible, it is always preferable to split the MI/MO model into a series of MI/SO models since the conditioning procedure of a large number of inputs and outputs [17] can introduce significant computational errors. In the present case, MI/SO models can be employed because the coupling between motions is principally due to the mechanical properties of the mooring system of the mini-TLP. These effects are included in the general excitation vector, $f(t)$. As mentioned earlier, it is preferable to consider the displacement and acceleration components as two different inputs so that there is no ambiguity in the determination of the mass and stiffness coefficients. Indeed, if only the displacements $q(t)$ are used as inputs to represent the linear path of the system, the mass and stiffness terms both appear in the real part of the same transfer function, which makes them impossible to discern. Utilizing the symmetry conditions of the mini-TLP and the assumption that only surge/pitch and sway/roll are the most important coupling effects, the 24-input/6-output MI/MO linear model can be recast as six MI/SO models, where each of these models requires either four (in the case of heave and yaw motions) or five (all the other modes of motion) different frequency response functions. As an example, the nonlinear model relating the five inputs to the longitudinal force is presented as a sum of linear sub-systems with the corresponding original transfer functions H_y in Fig. 1(a). Corresponding to this, Fig. 1(b) shows the linear sub-systems, the decoupled inputs and the linear transfer functions L_y, for the same problem.

If the measured inputs are not correlated to each other, the contribution of each input to the output can be obtained from the frequency response and ordinary coherence functions between the various inputs and the output. On the other hand, if the measured inputs are partially correlated, a new set of uncorrelated inputs must be obtained by conditioning the inputs before calculating the contribution of each input. To ensure that the conditioning analysis is successful, correct priorities of the correlated inputs must be determined somehow before conditioning. One reasonable approach is to put the correlated inputs in the order of their magnitude based upon the integral of the original coherence functions over a specified frequency range of interest.

2.4. Theoretical implementation

The theoretical formulation for determining the transfer functions using cross-spectral method [16] is presented here

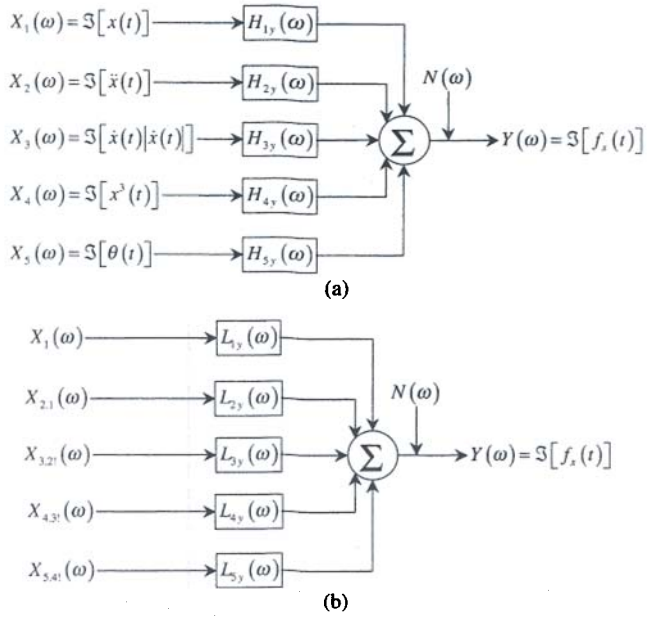

Fig. 1. Multiple input/single output models: (a) nonlinear system decomposed to linear sub-systems, and (b) linear sub-systems with decoupled inputs.

Table 1
Summary of MATLAB notations used in the text

MATLAB notation	Description
[,]	Horizontal concatenation
$1:1:N$	Is the same as $1,2,\ldots,N$
: (Used as index)	All the entries in that dimension
.*	Element-by-element product of the arrays
./	Element-by-element division of the arrays
.^s	Element powers if 's' is a scalar
shiftdim(X)	Shifts the dimensions of X
sum(X, dim)	Sum of the elements of X along dimension 'dim'
abs(X)	Absolute value of the elements of X.
prod(X, dim)	Product of the elements of X along dimension 'dim'
zeros(M, N)	Is an M-by-N matrix of zeros
size(X, dim)	Returns the length of the dimension of X specified by the scalar 'dim'

in a completely different format. The intent is to provide a different interpretation that other researchers may more easily assimilate in their work. In this section the equations are presented in a MATLAB format that is consistent with the writers implementation. Additional details regarding the MATLAB terminology used in this research are presented in Table 1 and a complete documentation can be found elsewhere [9]. For the R-MI/SO model, the N partially correlated inputs and the output time series are single column vectors of the same length n. The input vectors as well as the output vector are horizontally concatenated to produce a $n \times (N+1)$ two-dimensional matrix labeled X, where the output vector occupies the last column of the matrix. Note that at this point the order of the inputs does not matter, and that from this point on the text will refer to the columns of this matrix in a generic manner as vectors, without distinction between inputs and vectors contained within the matrix.

In order to organize the computations more efficiently, the auto- and cross-spectral densities are computed using the Welch method of spectral estimation and efficiently stored in a four-dimensional matrix labeled $S(i,j,f,k)$ with $i = 1:1:N+1$, $j = 1:1:N+1$, $f = 1:1:F$ and $k = 1:1:N+1$. The first and second dimensions (indices i and j) correspond to auto-spectral ($i = j$) and cross-spectral densities of vectors in X. The index for the third dimension, f, corresponds to the frequencies at which the spectral densities are estimated, and are linearly spaced between zero and the Nyquist frequency. The fourth dimension index, k, corresponds to the level of conditioning. Note that the auto- and cross-spectral densities of the unconditioned processes are saved in $S(i,j,:,1)$. The auto-spectral densities appear on the diagonal, while the cross-spectral densities appear off of the diagonal.

Following the computation of all the spectral densities of the unconditioned processes, the original coherence functions must be evaluated to assess the relative importance of the selected terms of the model. The original coherence functions are stored along the first row of a three-dimensional matrix labeled, C, indicated as

$$C(1,i,:) = ((\text{abs}(S(i,N+1,:,1))).\text{^}2)./(S(i,i,:,1). \times S(N+1,N+1,:,1)) \quad (10)$$

with $i = 1:1:N$. Next the inputs must be sorted in descending order along the second dimension of the matrix, X, according to the criteria mentioned in the previous section (the output vector still occupies the last column), and the process must be started over to ensure proper conditioning of the processes.

Using the matrix of unconditioned spectra, the initial transfer functions used in the conditioning procedure are evaluated using the following expression

$$L(1,j,:) = S(1,j,:,1)./S(1,1,:,1) \quad (11)$$

for $j = 2:1:N+1$. Then based upon Eq. (11) it is now possible to compute the conditioned auto-spectral densities, Eq. (12), cross-spectral densities, Eq. (13) and transfer functions, Eq. (14), sequentially, that is

$$S(i,i,:,k+1) = S(i,i,:,k) - (\text{abs}(L(k,i,:))).\text{^}2). \times S(k,k,:,k) \quad \text{if } j = i \quad (12)$$

$$S(i,j,:,k+1) = S(i,j,:,k) - L(k,j,:). \times S(i,k,:,k) \quad (13)$$

$$L(i,j, \quad = S(i,j,:,i)./S(i,i,:,i) \quad \text{if } i = k+1 \text{ and } j \geq i+1 \quad (14)$$

for $k = 1:1:N$, $i = k+1:1:N+1$ and $j = k+1:1:N+1$. The auto-spectral density obtained for the highest level of conditioning corresponds to the extraneous noise spectral density N, and is evaluated as

$$N = \text{shiftdim}(S(N+1,N+1,:,N+1)) \quad (15)$$

The computation of the Fourier transforms of the conditioned processes [15] is not necessary because the determination of the linear transfer functions of the conditioned system is a process that relies exclusively on the successive computation of the conditioned auto- and cross-spectral densities. Following the computation of all the conditioned spectral densities, the conditioned, cumulative and partial coherence functions must be examined to assess the goodness-of-fit of the selected model. The original function coherence can be computed using

$$C(1,j,:) = ((\text{abs}(S(i,N+1,:,1))).\text{^}2)./(S(i,i,:,1). \times S(N+1,N+1,:,1)) \quad (16)$$

with $i = 1:1:N$. The conditioned coherence functions can be conveniently stored in the same three-dimensional matrix C and is computed using

$$C(1,i,:) = ((\text{abs}(S(j,N+1,:,i))).\text{^}2)./(S(j,j,:,i). \times S(N+1,N+1,:,i)) \quad (17)$$

with $i = 2:1:N$ and $j = i:1:N$.

For convenience a two-dimensional matrix labeled, P, for the storage of intermediate results is introduced

$$P(:,i) = 1 - \text{shiftdim}(C(i,i,:)) \tag{18}$$

with $i = 1:1:N$. The cumulative coherence functions, Cc, are then determined consecutively using

$$\text{Cc}(:,i) = \quad - \text{prod}(P(:, \quad i), 2) \tag{19}$$

for $i = 1:1:N$. Adding a column of zeros to the left of Cc creates a matrix Ccz used for the computation of the partial coherence functions, Cp, as follows

$$\text{Ccz} = [\text{zeros}(\text{size}(\text{Cc}, 1), 1), \text{Cc}] \tag{20}$$

$$\text{Cp}(:,i) = \text{Ccz}(:,i+1) - \text{Ccz}(:,i) \tag{21}$$

for $i = 1:1:N$.

Finally, using the linear transfer functions of the conditioned system, L, the transfer functions of the original system, H, can be derived one after another by Eqs. (22)–(24), starting with Eq. (22)

$$H(:,N) = \text{shiftdim}(L(N, N+1, :)) \tag{22}$$

$$LH(:, j-i) = \text{shiftdim}(L(i,j,:)). \times H(:,j) \tag{23}$$

$$H(:,i) = \text{shiftdim}(L(i, N+1, :)) - \text{sum}(LH, 2) \tag{24}$$

for $i = N-1:-1:1$ and $j = i+1:1:N$. The original transfer functions, H, are the desired quantities of the conditioning and identifying procedure, from which the system frequency-dependent characteristics and model parameters can be retrieved by means of Eqs. (6)–(9).

3. Mini-TLP particulars

The mini-TLP was designed as an unmanned deepwater compliant platform for use off of West Africa [18]. In order for testing in a wider range of sea states the hull was modified including raising the elevation of the deck. Thus, the dynamic behavior is somewhat different than the original design and the sea states reported are somewhat different. As shown in Fig. 2, the mini-TLP hull consists of four vertical columns connected by four submerged rectangular pontoons. Other mini-TLP geometric and dynamic particulars of interest are summarized and presented in Table 2. The experiments were conducted using the 1:40 scale model [8]. All the results presented herein are reported at prototype scale. Both the rigidly constrained and compliant model tests were run with head and quartering sea platform orientations and the identical ocean wave simulations. For the rigidly constrained model tests, the mini-TLP hull was not fitted with either tethers or risers. The six DOF load cell was bolted to the model deck and to the access bridge as shown in Fig. 3. The load cell was carefully selected to provide adequate stiffness so that the vibrations were minimized at the testing frequency. The access bridge, which also can be used as a towing

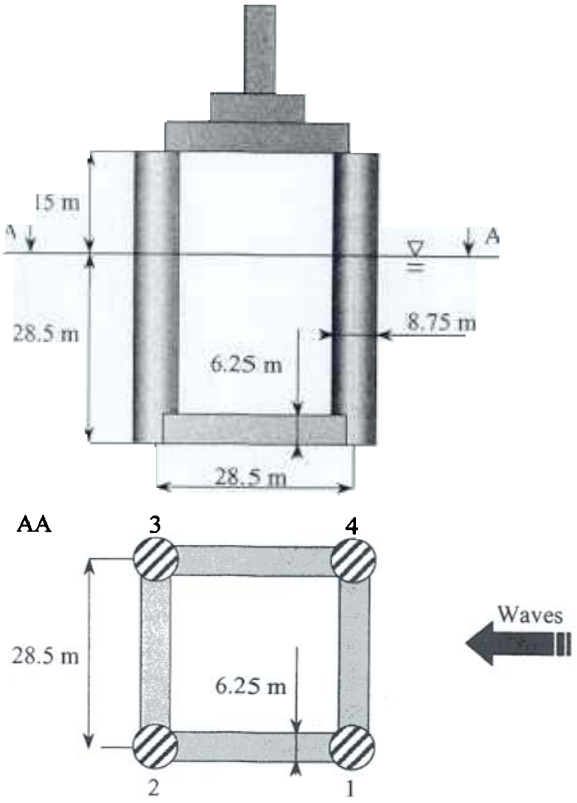

Fig. 2. Definition sketch of the mini-TLP hull configuration.

carriage, was lifted off its wheels and supported on blocks, and stiffened with installing adjustable bracing connected between bridge structure and the model basin walls. In an earlier set of tests, involving a truncated cylinder whose displaced mass was almost equivalent to that of the mini-TLP model, the dynamic amplification due to the load cell flexibility and system damping were evaluated. It was concluded that the inertial forces were negligible and that all the values in the cross-talk matrix of this instrument are less than five percent. Based upon evaluations from other earlier tests with the compliant model the mini-TLP was installed using an equivalent four-tethers/four riser system instead of the eight-tethers/twelve risers in the original design, see Fig. 4. The three restoring force components due to the tethers and risers at the connection points on the platform are computed using the top tensions and mini-TLP motions measured during the compliant model tests. The total restoring forces and moments are computed at the center of gravity of the platform and combined with the wave loads measured during the rigidly restrained hull tests to produce the components of the general excitation vector, $f(t)$.

The test program included a static offset test to demonstrate the stiffness behavior of the mooring system designed for the experiments. The results of this test indicated that the as-built system had been accurately scaled and provided restoring forces that were in accordance with the prototype specifications. Free-decay tests to determine

Table 2
Mini-TLP particulars used in the model test program

Properties	Prototype		Model	
	Full-scale value	Units	Equivalent full-scale value	Units
Water depth	1000	m	673.61	m
Total weight of mini-TLP	6620	mt	6445	mt
Vessel displacement	10,320	mt	10,158	mt
Tendon and riser pretension	3700	mt	3713	mt
Tendons axial stiffness	2.46×10^7	N/m	2.46×10^7	N/m
Risers axial stiffness	4.49×10^7	N/m	4.48×10^7	N/m
Center of gravity (X)	0	m	0	m
Center of gravity (Y)	0	m	0	m
Center of gravity (Z)	29.5	m	29.5	m
Pitch radius of gyration	21.5	m	21.7	m
Roll radius of gyration	21.5	m	21.9	m
Yaw radius of gyration	14	m	17.2	
Surge natural period	–	s	140 (0.007)	s (Hz)
Pitch natural period	4.9	s	4.6 (0.22)	s (Hz)
Heave natural period	2.6	s	2.8 (0.36)	s (Hz)
Sway natural period	–	s	136	
Roll natural period	4.9	s	4.56	
Yaw natural period		s	101	
Surge damping ratio		–	0.1927	
Sway damping ratio		–	0.1031	
Heave damping ratio		–	0.0077	
Pitch damping ratio		–	0.0166	
Roll damping ratio		–	0.0165	
Yaw damping ratio		–	0.0805	

natural periods and damping factors were also performed and the results are presented in Table 2. The mini-TLP was tested in specific design storm environments, as well as, several unanticipated storm environments for academic purposes. In the present study, only the data recorded during the simulations of the West Africa (JONSWAP spectrum with $H_s = 4$ m, $T_p = 16$ s and $\gamma = 2$) and Gulf of Mexico (JONSWAP spectrum with $H_s = 13.1$ m, $T_p = 14$ s and $\gamma = 2$) storms with the platform in head seas configuration will be used. The tests were recorded for 1707 s (three hours prototype scale) at a sampling frequency of 40 Hz (6.3246 Hz prototype scale) and filtered with a hardware low pass filter at 10 Hz (1.5811 Hz model scale). This resulted in records containing 68,280 data points in each time series.

4. Numerical applications of the R-MI/SO models

There are several important aspects of the R-MI/SO models that need to be examined using the mini-TLP data set. This includes the use and interpretation of the various coherence function concepts to understand the relative significance of each contribution to the response behavior by the various terms included in the equation models, the concept of extraneous noise, and the resolution of constant and frequency-dependent coefficients. Besides the recovery of coefficients, there is also the major issue of how to verify and interpret frequency-dependent results that are expected and those whose interpretation requires a deeper understanding of the portrayed physics behind the problem and the general interpretation of the R-MI/SO methodology.

In the results that follow the spectral densities, coherence functions and transfer functions were each computed at 200 frequencies between 0 and 0.3 Hz, corresponding to 0.015 Hz frequency spacing. A Hanning window to reduce leakage with a 50% overlapping was

Fig. 3. Rigidly restrained hull configured for quartering sea tests.

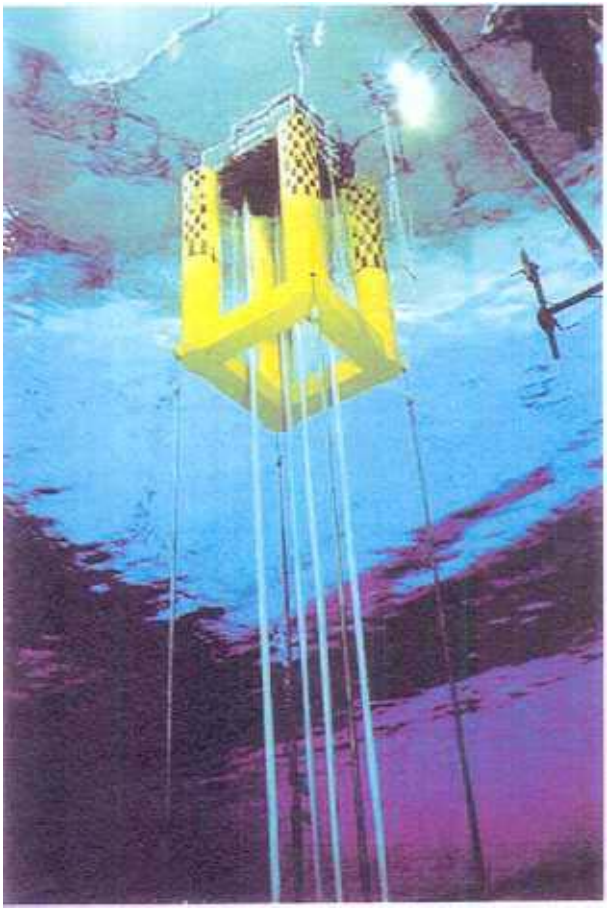

Fig. 4. Underwater photograph of the compliant mini-TLP, 4 tendons 4 risers, model configuration.

applied to the spectral analyses. A lowpass Butterworth filter with less than 3 dB of ripple in the pass band, defined from 0 to 0.3 Hz, and at least 40 dB of attenuation in the stop band, defined from 0.45 Hz to the Nyquist frequency (3.16 Hz), was designed to filter the time series. The numerical results presented focus upon the mini-TLP test data for the head seas configuration and the surge, heave and pitch response modes. The R-MI/SO model of which the output is the surge excitation force, $f_x(t)$, is used to illustrate the discussions on coherence functions and extraneous noise. Unless specified, this model will be used throughout the study for the identification of numerous parameters. Of course, the identification of parameters associated with other DOF requires the use of the R-MI/SO model of which the output corresponds to the same DOF excitation force (or moment). Fig. 5 presents the normalized auto-spectral densities of the West Africa wave excitation and the surge, heave and pitch platform responses. These graphs should only be viewed as providing information about the frequency content. In the wave frequency range, the surge excitation is slightly broader than the surge response because the wave forces measured on the rigid model are not exactly the same as the wave forces exerted on the compliant and the response spectral density of a nonlinear mechanical system is never proportional to the excitation spectral density. The pitch response exhibits two peaks; the second peak corresponds to the mini-TLP pitch natural period as reported in Table 2. The slow drift surge motion and heave set down are significant compared to the wave frequency motions.

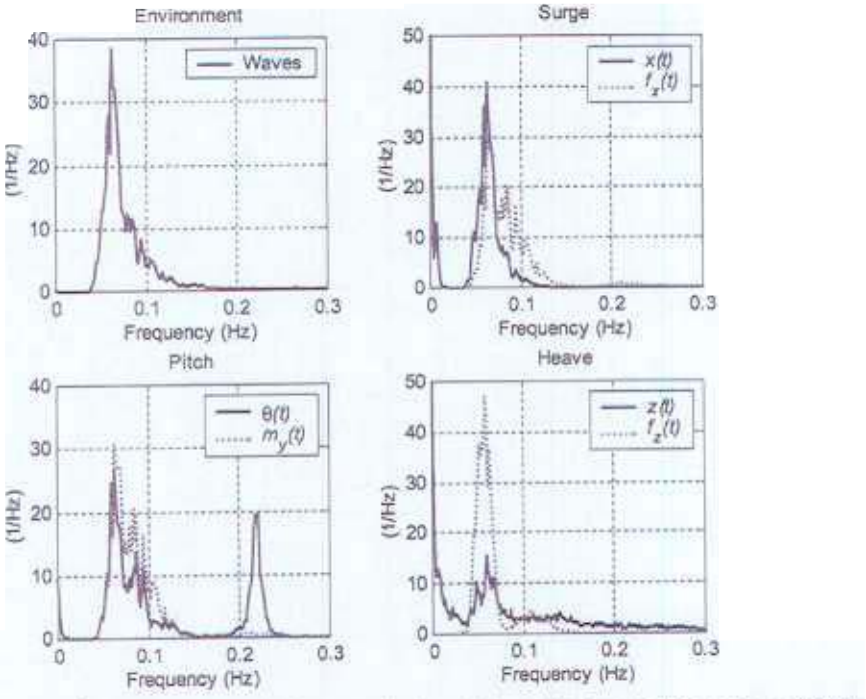

Fig. 5. Normalized auto-spectral densities of the design sea excitation and the resultant surge, pitch and heave responses

4.1. Coherence functions

The coherence functions are used in the beginning of the analysis to understand the relative importance of the various contributions to the response of the system being analyzed. The usual spectral evaluation of the coherence functions provides some insight into the various but not the relative significance of each input, however, the conditioned and cumulative coherence functions allows one to interpret the order of importance and significance of each of the terms in the coupled nonlinear system of equations.

In the R-MI/SO model of the mini-TLP of which the output is the surge excitation force, $f_x(t)$, the five inputs are, the surge displacement, the pitching rotation, the quadratic surge velocity, the heave displacement and the Duffing type cubic surge displacement. Fig. 6 presents the original coherence functions of these five inputs related to the surge excitation force, $f_x(t)$. In this figure, the five inputs have been sorted according to the order of magnitude of the integral of each individual coherence function in descending order of importance, as based upon the integral of each coherence function in the frequency range of interest, i.e. 0.03–0.17 Hz. The legend in Fig. 6 lists the inputs in decreasing order of priority and the two vertical dotted lines simply indicate the frequency range of interest. As mentioned earlier, the inputs are sorted according to the surface area bounded by each of the coherence function curves and the cutoff frequency lines. In the present case, the surface area can take any value between 0 and 0.14, which corresponds to the specified frequency bandwidth times the coherence of a perfectly correlated input. The magnitude of the integral of the five ordered inputs is, respectively, equal to 84, 76, 63, 38 and 37% of 0.14. These percentages do not add up because the original coherence functions do not satisfy the normality criterion. The priority of the inputs is dependent upon the specified frequency range of interest, and as in the implementation for this study, it is possible to vary the frequency range in the analysis procedure. For the present case, the choice of this frequency range was guided by the consideration of the overlapping sections of the excitation and response frequency ranges as shown in Fig. 5. Only the values of the parameters evaluated within this frequency range are considered to be reliable because the excitation energy outside this frequency range is negligible. The choice of the frequency range has a direct influence on the rest of the conditioning process and the final results.

The original coherence functions are also useful in the final stage of the identification process to locate the frequencies that exhibit high levels of coherence. It is useful then to introduce the concept of coherence threshold as a measure of confidence in the coefficient values identified by the R-MI/SO methodology. The system identification program developed for this study provides the flexibility to vary the values of the coherence threshold, and thus to select a value suitable by the researcher. For discussion purposes, a threshold of 0.75 was selected. To aid in the graphical interpretation of the data, special markers were attached at each frequency where the value of the variable of interest had a coherence value greater than or equal to this threshold value.

It has been recognized that the original coherence functions cannot be used to adequately assess the contribution of each input to the system model [16], rather for this purpose the partial and cumulative coherence functions are introduced. These coherences are based upon

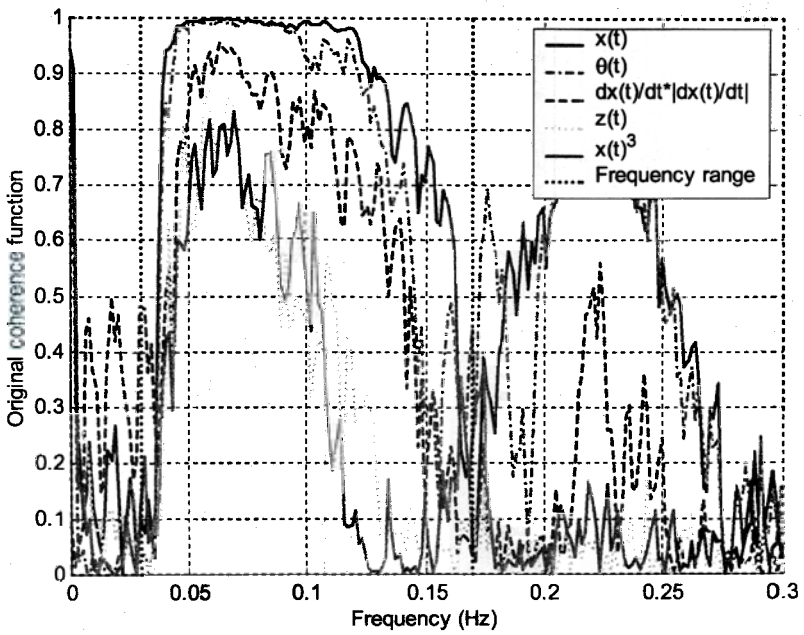

Fig. 6. Original coherence functions for the R-MI/SO model using the inline force, $f_x(t)$, as output

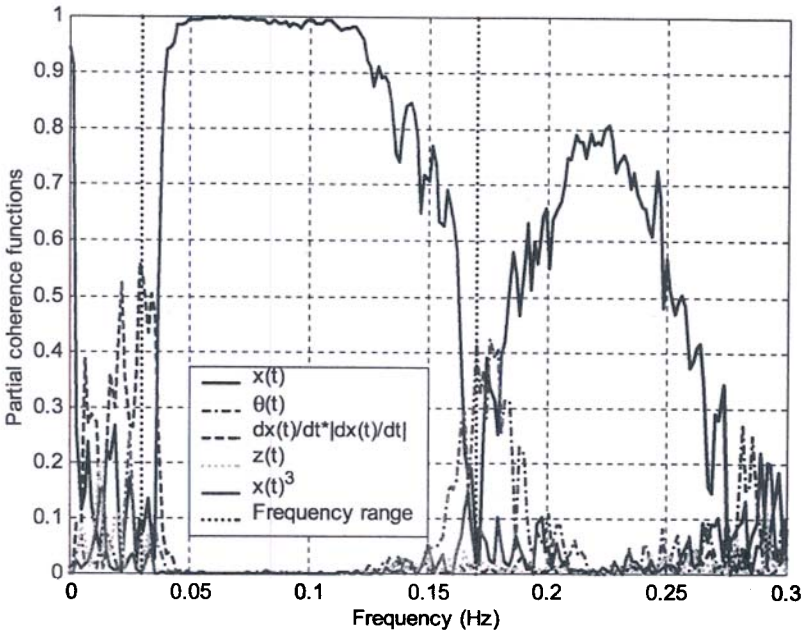

Fig. 7. Partial coherence functions for the R-MI/SO model using the inline force, $f_x(t)$, as output.

the conditioning of the input spectrum and accurately reflect the importance of each input contribution to the response. The partial coherence values for the five inputs are presented in Fig. 7. The most important feature that can be observed is the near unity value of the linear component's partial coherence function. This indicates that most of the output, $f_x(t)$, auto-spectral density can be accounted for by the surge input, $x(t)$. Fig. 8 presents the cumulative coherence function and it reflects the goodness of the selected model in describing the physical system. This graph is used to show how the cumulative coherence function is improved by including additional terms. In this case the cumulative coherence function closely follows the fluctuations of the surge partial coherence function. This suggests that the addition of any other terms in the governing equations would not significantly improve the model. By considering the wave spectrum excitation frequency range, as shown in Fig. 5, it can be observed that in the region of high energy content that coherence functions are generally well resolved. However, outside that region the signal to noise ratio degrades and the coherence falls rapidly. The variations shown in the extraneous noise spectrum presented in Fig. 9 are also consistent with this observation.

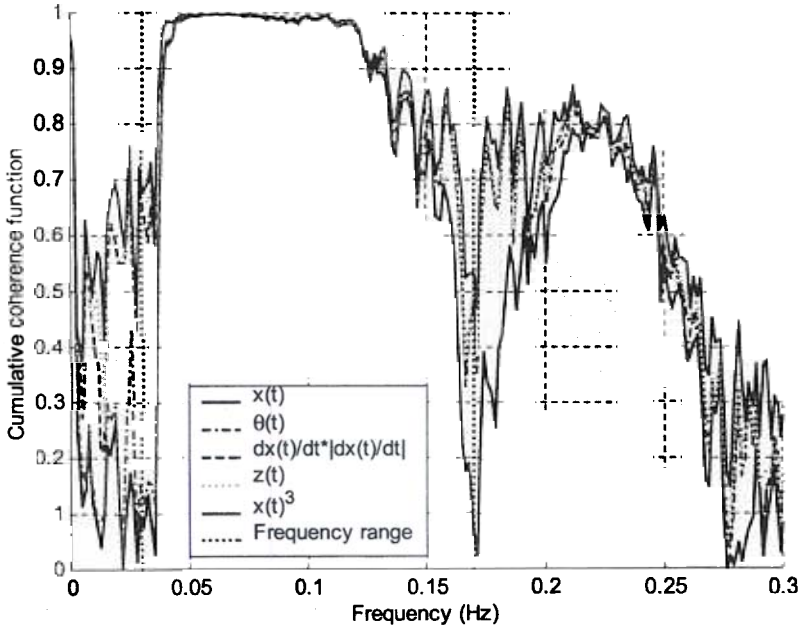

Fig. 8. Cumulative coherence functions for the R-MI/SO model using the inline force, $f_x(t)$, as output.

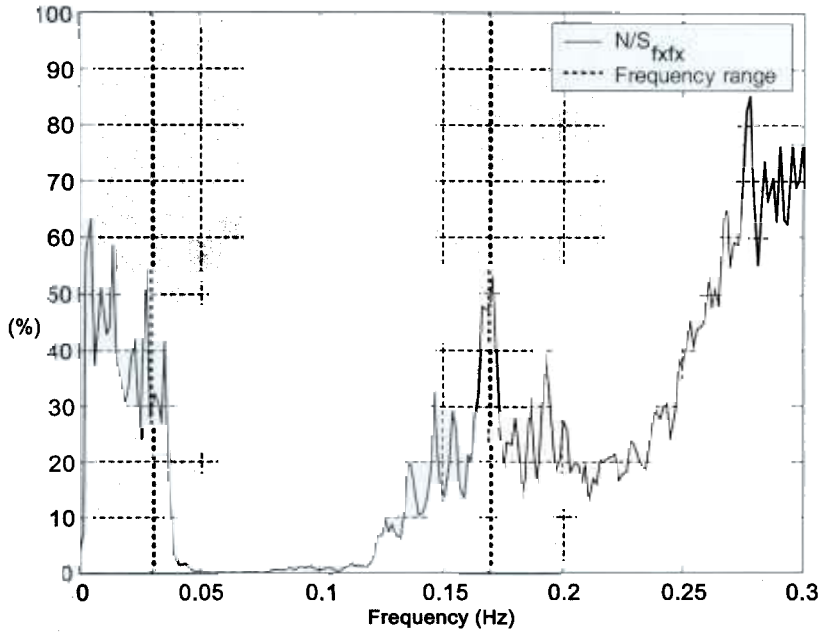

Fig. 9. Extraneous noise for the R-MI/SO model using the inline force, $f_x(t)$, as output.

4.2. Extraneous noise

The noise content in the recorded time series is assumed to be introduced either during measurement or the signal processing of the data, and hence, the terminology of extraneous noise. It follows then that the noise is assumed to be independent of the system inputs and output. The spectral density of the extraneous noise to signal ratio is presented in Fig. 9. This figure provides a better indication of the amount of extraneous noise in the system than if one were simply to present the extraneous noise spectral density by itself. For this figure it can be verified that the R-MI/SO methodology provides a means to evaluate whether the optimum integrodifferential equation describing the system has been found that minimizes the extraneous output noise. In Fig. 9, it is seen that in the frequency region of 0.04–0.13 Hz that the extraneous noise represents less than 10% of the output signal. Outside of this frequency range in the frequency bands between 0.03–0.04 and 0.13–0.17 Hz the extraneous noise is significant and one can expect that coefficients identified in these range will not be accurate.

4.3. Frequency-dependent added-mass and damping coefficients

The frequency dependence of the hydrodynamic added-mass and damping coefficients affects considerably the dynamic response of floating platforms. Offshore engineers have paid an increasing attention to this phenomenon over the past decade by putting their efforts in the development of numerical tools that can accurately predict the nonlinear hydrodynamic response behavior of deepwater structures. In order to validate the R-MI/SO results identified from experimental data for these coefficients, the results will be compared directly with the numerical predictions of the industry standard radiation–diffraction panel code WAMIT® [19].

A three-dimensional mesh of the mini-TLP hull with 2856 panels was created. Two planes of symmetry were used thus reducing the number of panels required to 714 panels for the single quadrant; other options are available for the more advanced hydrodynamic modeler [19]. The origin of the coordinate system was located at the intersection of the undisturbed free surface and the two planes of symmetry and the characteristic length was set equal to 4.375 m, which corresponds to the radius of the columns. In the force control file, the horizontal modes (surge, sway and yaw) were free and the vertical modes (heave, pitch and roll) were fixed, to represent a TLP moored by vertical tethers. The mini-TLP was simulated in a finite water depth of 673.6 m. The added-mass and damping coefficients were evaluated at 43 periods between 0.005 and 0.3 Hz. The volume of the hull evaluated using WAMIT was equal to 9888 m^3. This volume multiplied by the density of seawater is equal to 10,155 mt and is within 3 mt of the full-scale equivalent model displacement reported in Table 2.

The identified structural mass, m, and surge added-mass, a_{11}, together with the numerical predictions are presented in Fig. 10. The value of the identified structural mass plus added-mass averaged over the frequency range of 0.03–0.11 Hz is quite reasonable. At 0.11 Hz, the identified parameter begins to decrease; the added-mass becomes negative when the identified parameter crosses the dashed line of the known structural mass whereas the predicted added-mass coefficient remains approximately constant over the whole frequency range. Although the numerically predicted added-mass remains positive, it has been

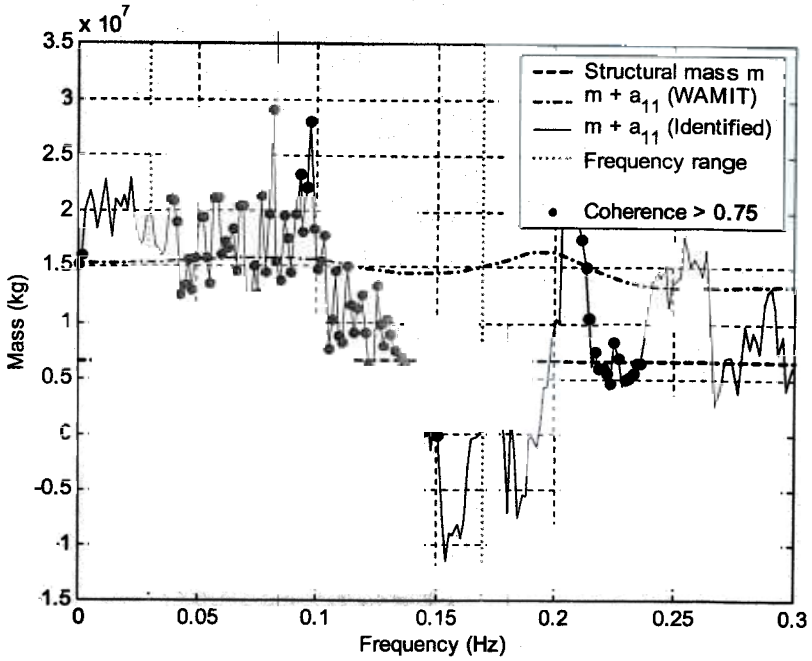

Fig. 10. Comparison of the structural mass, m, and the frequency-dependent surge added-mass, a_{11}

demonstrated that for certain parameter combinations, a freely floating compound cylinder could also exhibit negative values for the surge added-mass over specific frequency ranges [20]. An attempt to understand the high coherence values in the [0.21 Hz, 0.235 Hz] frequency range was investigated by shifting the specified frequency range in the analysis procedure to cover that range. Fig. 11 shows that the priority of the main inputs remains unchanged. Consequently, Fig. 12 is comparable to Fig. 10; the identified surge added-mass does not change significantly. However, there is a noticeable link between this [0.21 Hz, 0.235 Hz] frequency range and the second peak of the pitch auto-spectral density shown in Fig. 5. The identified coupled surge/pitch added-mass, a_{15}, is presented in Fig. 13. The R-MI/SO model results and numerical predictions have surprisingly comparable trends throughout the whole frequency range, and within the frequency range of interest, the two evaluations have the same order of magnitude.

In order to identify the pitch moment of inertia, I_{yy}, and pitch added-mass, a_{55}, the R-MI/SO model of which the output is the pitch moment excitation, $m_y(t)$, is

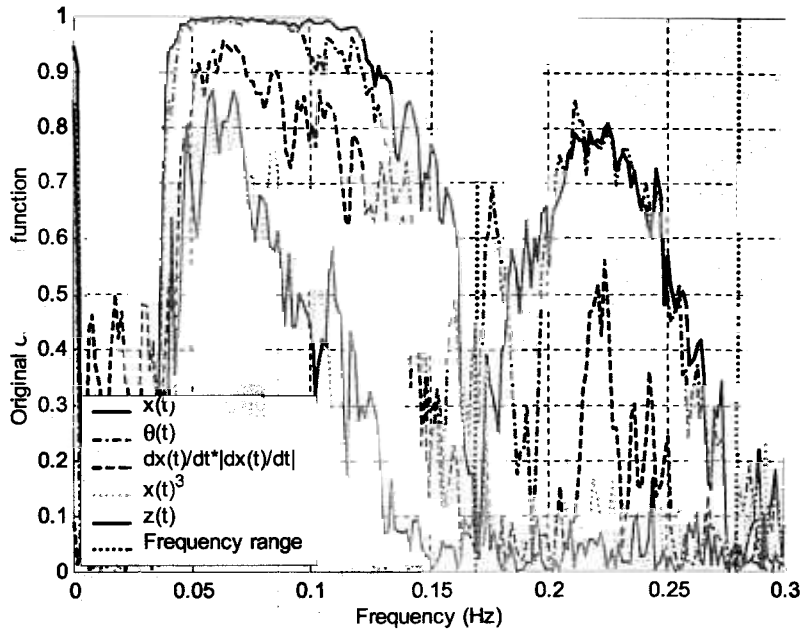

Fig. 11. Original coherence functions for the R-MI/SO model using the inline force, $f_x(t)$, as output, for a different specified frequency range.

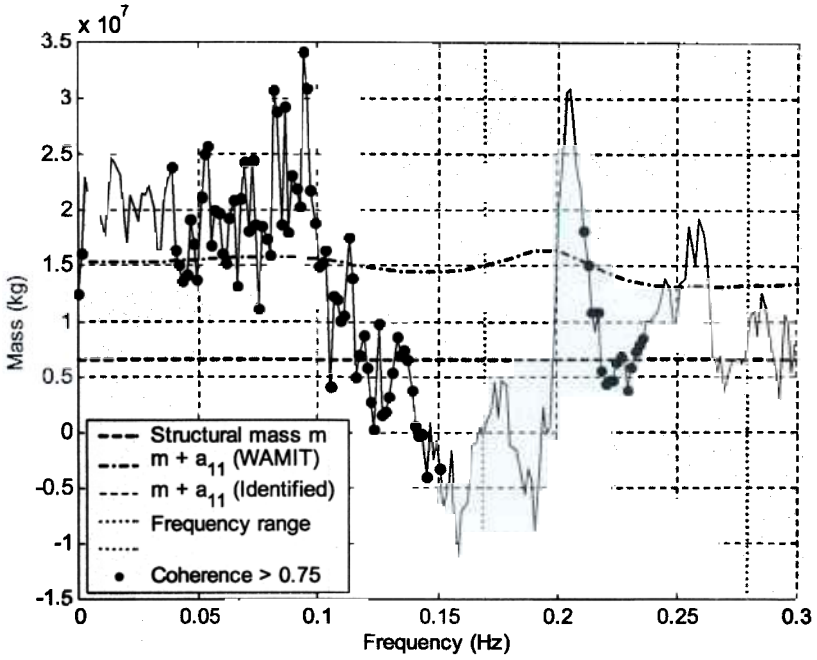

Fig. 12. Comparison of the structural mass, m, and the frequency-dependent surge added-mass, a_{11}, for a different specified frequency range.

considered. The identified moment of inertia I_{yy} and pitch added-mass, a_{55}, are presented in Fig. 14. The first parameter is identified using the R-MI/SO model relative to $m_y(t)$, the pitch angular moment. The value of the identified parameter averaged over the frequency range is roughly equal to the pitch moment of inertia $I_{yy} = 3.035 \times 10^9$ kg m^2, which can easily be obtained from the known pitch radius of gyration and structural mass. The pitch added-mass, a_{55}, is not recovered by this methodology. This is probably a confirmation that the platform is designed for small pitch rotations. For a severe wave environment produced in a 100-year Gulf of Mexico storm the mini-TLP exhibited pitch rotations between -2.8408 and 2.8845°, with a standard deviation of 0.4498°. Another possible reason for the inability to correctly identify the sum of both parameters could be that the level of accuracy of measurements was close to the limits of the instrumentation.

The structural mass, m, and heave added-mass, a_{33}, are predicted using the R-MI/SO model that yields the vertical

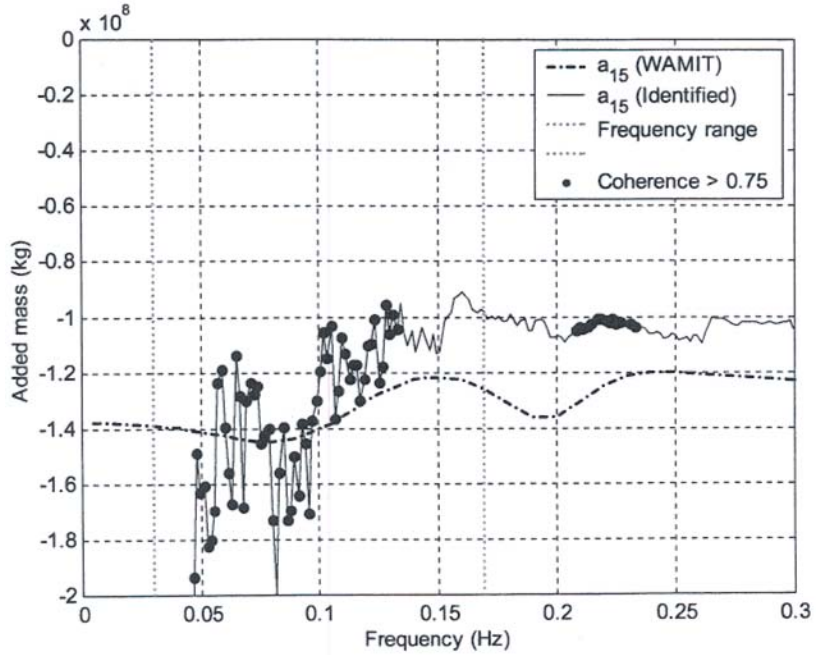

Fig. 13. Comparison of the frequency-dependent coupled surge/pitch added-mass, a_{15}.

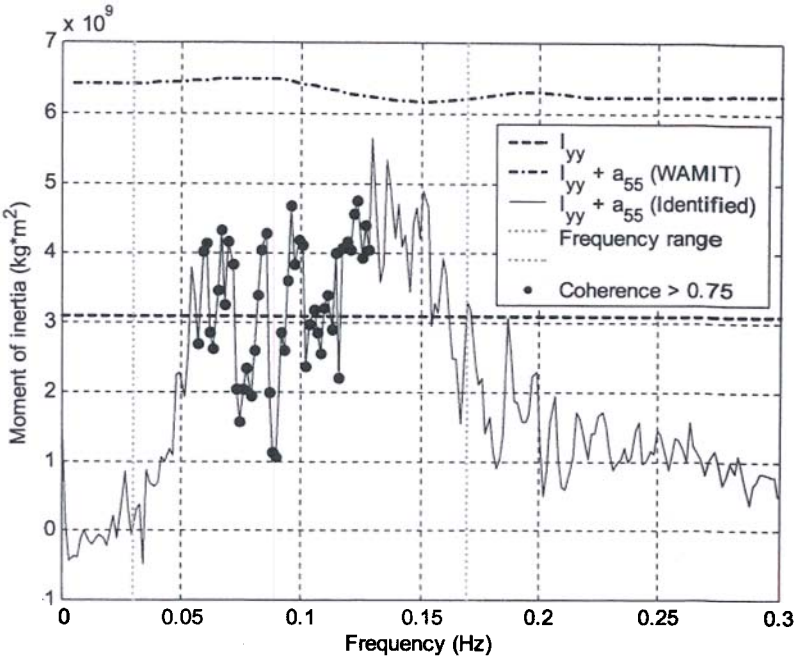

Fig. 14. Comparison of the pitch moment of inertia, I_{yy}, and the frequency-dependent pitch added-mass, a_{55}.

force excitation, $f_z(t)$, as output. The identified structural mass, m, and heave added-mass a_{33}, predictions are presented in Fig. 15. Based upon similar reasoning this probably explains why the heave added-mass a_{33} is not well recovered by the methodology. The mini-TLP mooring system consists of vertical taut tethers designed to minimize the heave motions. The maximum and minimum heave motions are, respectively, 0.2916 and −0.3881 ft, the standard deviation is equal to 0.0692 ft. The variations of the identified parameter are affected by the frequency distribution of the wave excitation. Although the identified value of this parameter is not reliable, the numerical prediction is consistent with published findings [5]. In that study it was found that at deep submergence of $s/a = 8.0$ in infinite depth, which approximately corresponds to the mini-TLP setup, the measured heave added-mass coefficient is nearly constant.

The identified surge linear damping, b_{11}, and the numerical predictions are presented in Fig. 16. In this case the agreement between the two procedures is excellent in

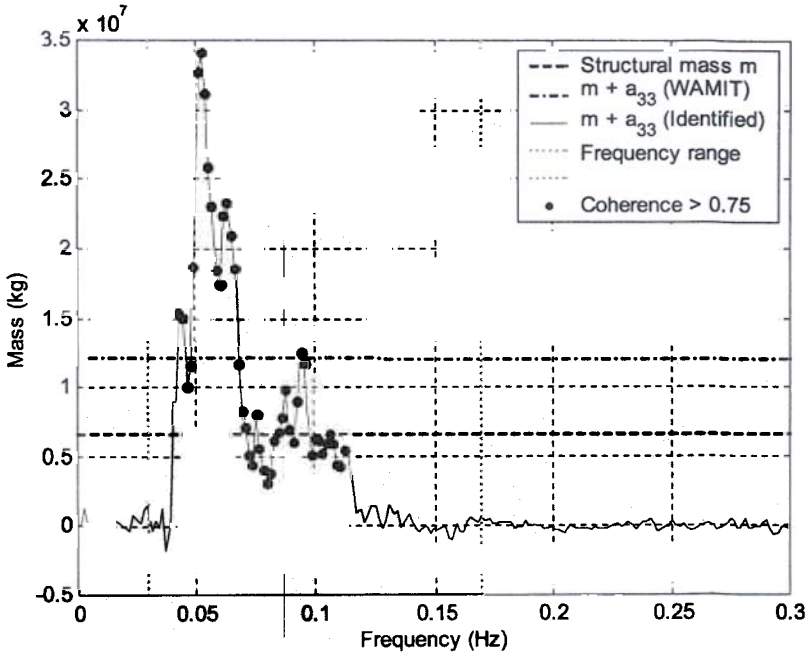

Fig. 15. Comparison of the structural mass, m, and the frequency-dependent heave added-mass, a_{33}.

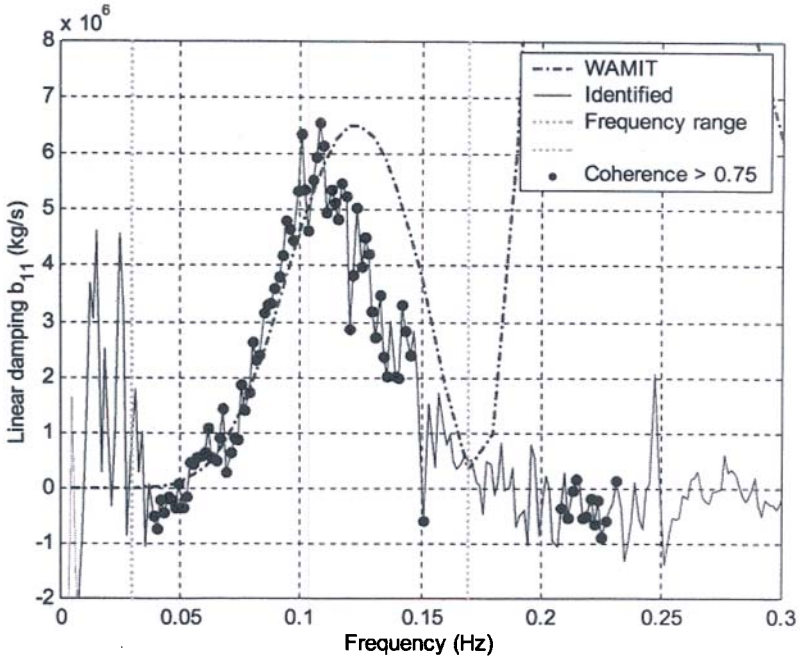

Fig. 16. Comparison of the frequency-dependent surge linear damping, b_{11}.

the [0.04 Hz, 0.11 Hz] frequency range where the largest amount of energy is dissipated by the system through its surge motion. The surge linear damping coefficient computed using the damping ratio reported in Table 2 is equal to 9.75×10^6 kg/s. This value is greater than the results obtained but nonetheless of the same order of magnitude.

4.4. Linear surge and heave stiffness

The identified linear stiffness, k_{11}, is presented in Fig. 17. The linear stiffness identified at frequencies close to 0 Hz agrees very well with the result of the offset test performed in calm water where the linear trend line for

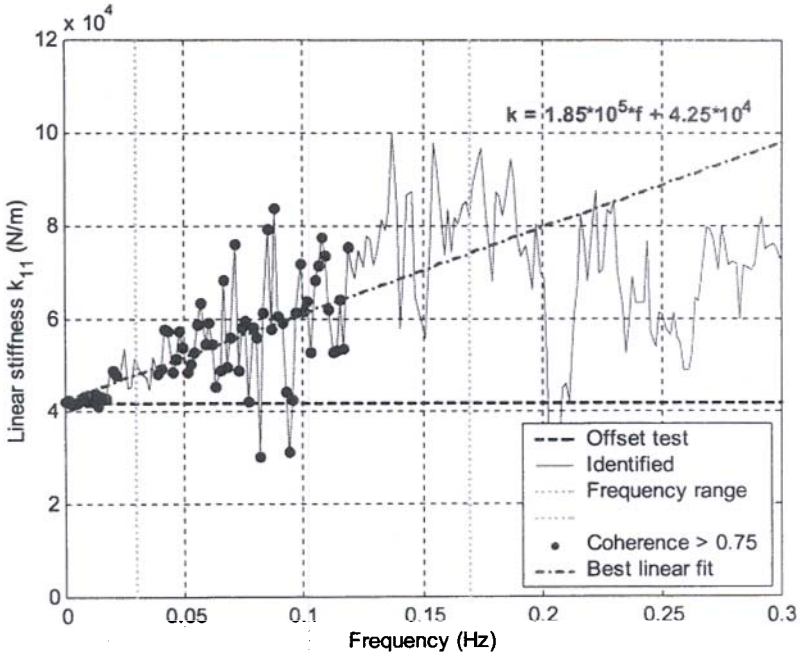

Fig. 17. Comparison of the frequency-dependent surge linear stiffness, k_{11}.

the specified stiffness to surge offset had a slope of 4.2×10^4 N/m. In the present case, the identified parameter is not constant but displays a well-defined pattern: the linear stiffness increases in a seemingly linear manner as the frequency increases up to 0.15 Hz. Using a linear fit over that frequency range, the proportionality constant was estimated to 1.85×10^5 Ns/m. The most likely physical explanation of this phenomenon is that wave frequency motions have effects on a shorter length of tethers than slow-drift motions. At low frequencies, the tethers respond linearly from their anchors to their connections on the platform hull, and at higher frequencies the transverse drag force on the tethers keeps them relatively straight over most of the water column, while only the upper portion of the tethers moves. The decreased length of the tethers freely moving contributes to a virtual increase of the linear surge stiffness.

Similarly to the heave added-mass, the linear heave stiffness, k_{33}, is predicted using the R-MI/SO model that yields the vertical force excitation, $f_z(t)$, as output. The identified linear heave stiffness, k_{33}, is presented in Fig. 18. Although the scatter is consequential, the averaged value of the data points of high coherence matches the total stiffness of the tethers and risers 6.95×10^7 N/m, displayed as a dashed line.

4.5. Nonlinear stiffness and damping

This last example deals with hypothesized nonlinear terms that might be important to the problem are used to illustrate the ability of the R-MI/SO technique to handle additional nonlinear terms, assess their contributions to the selected model and capture the frequency dependence of any type of term. In this study, a cubic Duffing type stiffness term and a quadratic damping term have been arbitrarily included in the problem statement since they are both reasonable types of nonlinearities for offshore engineering problems.

The identified nonlinear stiffness, r_{11}, is presented in Fig. 19. This identified parameter exhibits unusual frequency dependence. In this case no numerical benchmarking is available to verify the frequency dependence, nor the magnitude of this parameter. In cases like this, one must resort to other means to try and interpret the reliability of this result. First, it can be observed that there are only a small number of markers indicating values of high coherence. This suggests that the particular nonlinearity provides a negligible contribution to the model. Broadly speaking, when an identified parameter exhibits unusual frequency dependence, special caution must be exercised in the interpretation of the parameter's contribution to the model. Either the model is incorrect, or the particular frequency dependence is associated with complex physical aspects.

The identified nonlinear damping, d_{11}, is presented in Fig. 20. The polynomial fit of the values of high coherence indicates a clear frequency dependence of the nonlinear damping. This result at first seems to contradict the hypothesis made in a recent research study [7], which still constituted a significant advancement by proving the importance of the frequency dependence of the added-mass and damping coefficients in the simulation of nonlinear ship rolling. Indeed, in order to compare their extended state space model with full-scale experimental data, an additional nonlinear damping term had to be added to the wave damping. Since nonlinear terms cannot be included in extended state space approximations due to

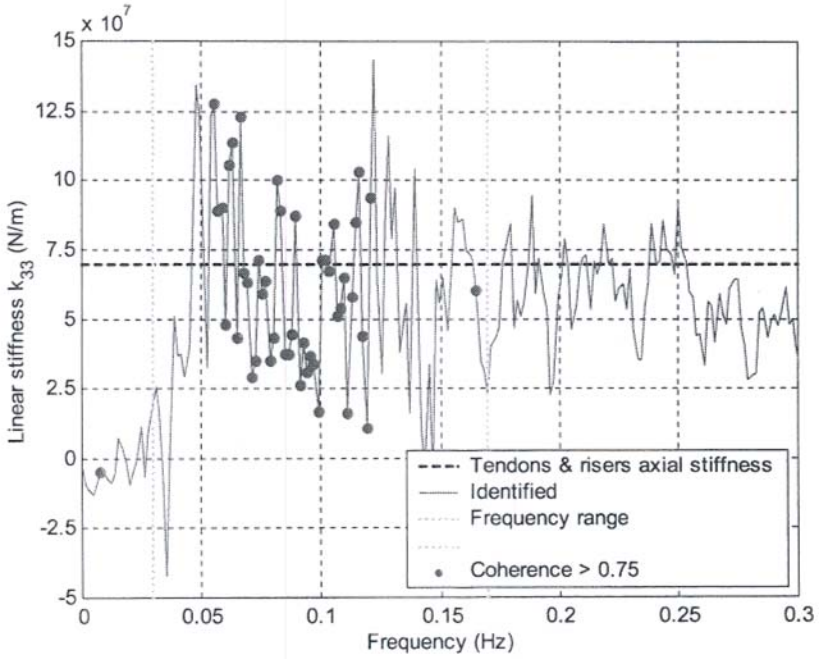

Fig. 18. Comparison of the frequency-dependent heave linear stiffness k_{33}.

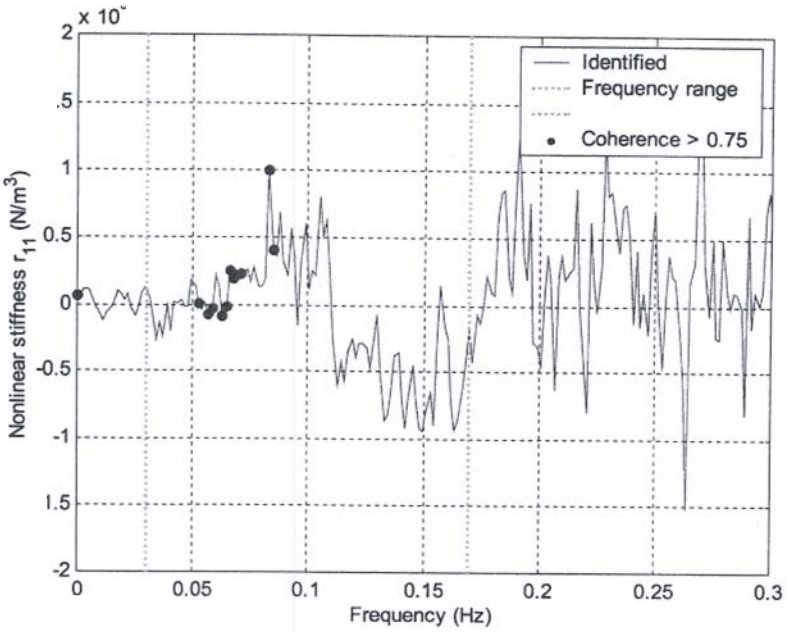

Fig. 19. Frequency-dependent surge nonlinear stiffness, r_1

linearity requirement of the model, the nonlinear term was merely assumed to be constant over the frequency range. In this study, the application of the R-MI/SO method makes no restrictive assumption about the parameters and the frequency dependence of the nonlinear damping is illustrated.

5. Summary and conclusions

In this research study, the R-MI/SO technique based upon the work of Bendat [1,2] is used in combination with the dynamic response model of a compliant offshore structure for the identification of the system parameters from real excitation and response data. The environmental excitation was limited to only waves with the expectation that the system would behave as a weakly nonlinear system. The form of the mathematical model is initially built upon the known mechanical properties of the system. Next, by means of the computation of the original coherence functions between each potential input and the output, the most relevant inputs are selected and retained for the identification of the related parameters. The comparison of the inputs' original coherence functions within a specified

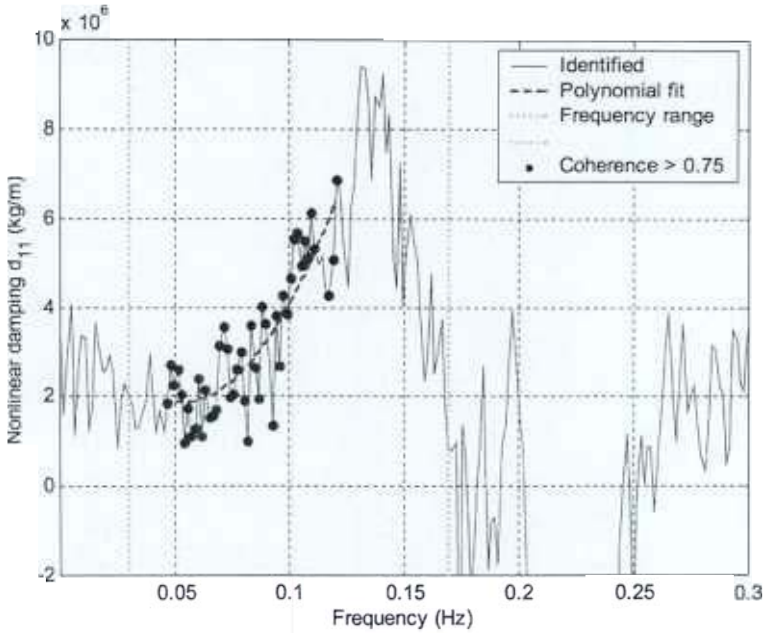

Fig. 20. Frequency-dependent surge nonlinear damping, d_1

frequency range is used for the sorting of the inputs before applying the conditioning procedure leading to the transfer functions, from which the system frequency-dependent characteristics and model parameters are retrieved. The completeness of the model is achieved by monitoring the increase of the cumulative coherence functions and the decrease of the extraneous noise spectrum over the frequency range of interest when additional terms are included. In the present case, the dynamic response model takes into account the most important mode couplings as well as Duffing type stiffness and quadratic damping nonlinearities.

The results obtained confirm the correctness of the model and demonstrate a strong consistency for the model related to surge motions, which is the predominant mode of motion of tension leg platforms in uni-directional sea states. The identified value of all the parameters included herein is satisfactory for the specific range of parameters considered and the conditions in which the input and output signals to the R-MI/SO model were recorded. The value of parameters such as the heave linear stiffness recovered via spectral averaging of the respective transfer function compares favorably to the known constant value. The identification of frequency-dependent parameters, such as the surge and surge/pitch added-mass or the surge linear damping coefficient, proved to be quite accurate and in good agreement with the numerical WAMIT predictions around the excitation peak frequency. The identified value of the heave linear stiffness proved to be correct for the static case and interestingly exhibited a linear trend increasing as a function of frequency. This would not have been picked up without the implementation of a process to ensure the partition of the parameters. The recovery of the nonlinear stiffness coefficient showed that no significant error is introduced by including additional linear or nonlinear terms which contribution is negligible since the identified value of the term is approximately zero. Conversely, if one does not include sufficient terms the cumulative coherence functions will provide some guidance in choosing correctly the additional terms. It was reasoned for this study that the cause why some parameters were poorly recovered is that the particular design of the mini-TLP minimizes the motions related to these parameters, therefore making the identification process somewhat difficult. Apparently, this finding is consistent with system identification techniques in general and it is only a minor shortcoming as only the parameters associated with the largest motions are of real interest.

Of course, great caution must be exercised in generalizing these results beyond what has been done. Parameters evaluation is likely to be strongly influenced by the spectral characteristics of the loads used for excitation of the system. Perhaps the results could be improved if a band-limited white noise was used to persistently excite the system in the laboratory. However, using band-limited white noise excitation for the purpose of system identification is a debatable issue when dealing with real engineering applications, in view of the fact that only data due to environmental excitation can be collected in the field. Furthermore, improvements would also be significant if the kinematics and loads were measured during the same tests. Bearing this in mind and the fact that measured experimental data were used, for many of the variables a reasonable level of agreement was obtained for the identified variables over the frequency range of interest. Based upon the results obtained in this study it is apparent that the nearly perfect agreement for numerically simulated data as shown in other research investigations [16], should not be expected when analyzing measured data.

Broadly speaking, this research study shows that no parameter can be assumed constant unless its identified value follows a horizontal line over a certain frequency range. The R-MI/SO technique is a very powerful tool for identification of frequency-dependent parameters in complex offshore engineering systems. As long as the system studied can be reasonably modeled by means of a nonlinear differential equation, the R-MI/SO technique is preferable to Volterra methods that require large amounts of data, which are not generally available in most measurement programs. Although the application of this procedure to ships and other offshore platforms is straightforward, one can expect to observe unexpected results and this study provides some insight as to how one might approach the solutions.

Acknowledgements

The writers gratefully acknowledge the partial financial support of the Offshore Technology Research Center, Statoil Norway and the Minerals Management Service during this study and express special thanks to Dr Per Teigen (Statoil) for his technical assistance during the mini-TLP model tests as well as providing the mesh used in some of the numerical simulations. The second writer also would like to recognize the partial support of the R.P. Gregory '32 chair endowment during this study. The writers are also pleased to acknowledge the insightful and constructive comments by the anonymous reviewers, including bringing a recent and relevant conference article to our attention.

References

[1] Bendat JS. Nonlinear system analysis and identification from random data. New York: Wiley/Interscience; 1990.

[2] Bendat JS. Nonlinear systems techniques and applications. New York: Wiley/Interscience; 1998.

[3] Bendat JS, Coppolino RN, Palo PA. Identification of physical parameters with memory in non-linear systems. Int J Non-Linear Mech 1995;30(6):841–60.

[4] Bhattacharyya SK, Panneer Selvam R. Parameter identification of a large floating body in random ocean waves by reverse MISO method. Proceedings of 20th Offshore Mechanics and Arctic Engineering Conference, 2001. p. 211–6.

[5] Chung JS, Kim MH. Added-mass and damping on an oscillating surface-piercing column with a horizontal cylinder: square cross sections. Int J Offshore Polar Engng 1995;5(3):595–602.

[6] Faltinsen OM. Sea loads on ships and offshore structures. UK: Cambridge University Press; 1990.

[7] Holappa KW, Falzarano JM. Application of extended state space to nonlinear ship rolling. J Ocean Engng 1999;24:47–58.

[8] Liagre PF, Guichard A. Mini-TLP test program. Offshore Technology Research Center Report. College Station, Texas: Texas A&M University; 2000.

[9] MATLAB®, The language of technical computing. Release 12.1. The Mathworks, Inc; 2001.

[10] Mulk MT, Falzarano JM. Complete six-degrees-of-freedom nonlinear ship rolling motion. J Offshore Mech Artic Engng 1994; 116:191–201.

[11] Narayanan S, Yim SCS. Nonlinear model evaluation via system identification of a moored structural system. Proceedings of the 10th International Offshore and Polar Engineering Conference, 1998.

[12] Newman JN. Marine hydrodynamics. Cambridge, MA: MIT Press; 1977.

[13] Niedzwecki JM, Liagre PYF. System identification of distributed-parameter marine riser models. J Ocean Engng 2002.

[14] Niedzwecki JM, Liagre PF, Borgman LE, Teigen P. Directional sea response of a mini-TLP. Proc 11th Int Offshore Polar Engng Conf 2001;1:425–47.

[15] Panneer Selvam R, Bhattacharyya SK. Parameter identification of a compliant nonlinear SDOF system in random ocean waves by reverse MISO method. J Ocean Engng 2001;28:1199–223.

[16] Spanos PD, Lu R. Nonlinear system identification in offshore structural reliability. J Offshore Mech Artic Engng 1995;117(3): 171–7.

[17] Sridhar JK, Mulder JA, van Staveren WHJJ. Compact representation of multiple input/single output (MIMO) algorithms with applications to helicopter flight data. Proceedings of the American Control Conference, Baltimore, Maryland, 1994.

[18] Teigen P, Niedzwecki JM. Experimental and numerical assessment of mini-TLP for benign environments. Proceedings of the 8th International Offshore and Polar Engineering Conference, Montreal, Canada, 1998.

[19] WAMIT®. User Manual. Versions 5.4, 5.4PC, 5.3S. WAMIT, Inc; 1999.

[20] Williams AN, Li W. The hydrodynamics of floating compound cylinders. J Offshore Mech Artic Engng 1999;121: 213–8.